

Classification of crystalline topological semimetals with an application to Na₃Bi

Ching-Kai Chiu

Department of Physics and Astronomy, University of British Columbia, Vancouver, BC,
Canada V6T 1Z1
Quantum Matter Institute, University of British Columbia, Vancouver BC, Canada V6T 1Z4
E-mail: chiu7@phas.ubc.ca

Andreas P. Schnyder

Max-Planck-Institut für Festkörperforschung, Heißenbergstrasse 1, D-70569 Stuttgart,
Germany
E-mail: a.schnyder@fkf.mpg.de

Abstract. Topological phases can not only be protected by internal symmetries (e.g., time-reversal symmetry), but also by crystalline symmetries, such as reflection or rotation symmetry. Recently a complete topological classification of reflection symmetric insulators, superconductors, nodal semimetals, and nodal superconductors has been established. In this article, after a brief review of the classification of reflection-symmetry-protected semimetals and nodal superconductors, we discuss an example of a three-dimensional topological Dirac semimetal, which exhibits time-reversal symmetry as well as reflection and rotation symmetries. We compute the surface state spectrum of this Dirac semimetal and identify the crystal lattice symmetries that lead to the protection of the surface states. We discuss the implications of our findings for the stability of the Fermi arc surface states of the Dirac material Na₃Bi. Our analysis suggests that the Fermi arc of Na₃Bi is gapped except at time-reversal invariant surface momenta, which is in agreement with recent photoemission measurements.

1. Introduction

Finding new topological materials beyond the Bi-based topological insulators has become an important goal in solid state research. In the past few years, it has been realized that not only internal symmetries [1, 2, 3, 4, 5], such as time-reversal, but also crystal symmetries, for example crystal reflection or rotation, can lead to the protection of topological states [6, 7, 8, 9, 10, 11, 12, 13, 14, 15, 16, 17]. In fact, a complete classification of reflection-symmetry-protected insulators and fully gapped superconductors was recently presented in Refs. [15, 16, 17]. The topological character of these crystalline topological insulators and superconductors gives rise to gapless states at the boundary. Importantly, since the surface of a material has lower crystal symmetry than its bulk, not all surfaces of a crystalline topological insulator (or superconductor) exhibit gapless boundary states. Only those surfaces that are invariant under the crystal symmetry can support topological surface states. Experimentally, SnTe has been identified to be a crystalline topological insulator with Dirac cone surface



states, that are protected against gap opening by reflection symmetry together with time-reversal symmetry [18, 19, 20, 21]. Other candidate materials for reflection-symmetry-protected topological insulators are the anti-perovskites Ca_3PbO and Sr_3PbO [22, 23, 24].

The concept of topological band theory can also be applied to nodal systems, such as semimetals and nodal superconductors. The stability of the Fermi surfaces (superconducting nodes) of these materials is ensured by the conservation of a topological invariant which is defined in terms of an integral along a contour enclosing (encircling) the Fermi point (Fermi line). Topological nodal systems can be protected by global symmetries [25, 26, 27, 28, 29, 30, 31, 32, 33] (i.e., internal symmetries, such as time-reversal) as well as crystal lattice symmetries, or a combination of the two [34, 35, 36, 37, 38]. The nontrivial topology of the electronic band structure of these gapless materials manifests itself at the boundary in terms of protected surface states. Depending on the symmetry properties and the dimension of the Fermi surface, these surface states form Dirac cones, flat bands, or Fermi arc states [30]. Recently, several materials have been experimentally identified to be crystal-symmetry-protected topological semimetals. Among them are the Dirac materials Cd_3As_2 [39, 40, 41, 42, 43, 44, 45] and Na_3Bi [46, 47, 48, 49], whose Dirac points are protected by rotation symmetry. The Fermi arc states of Na_3Bi have recently been observed in angle-resolved photoemission measurements [48, 49].

In this paper, we first present in Sec. 2 a short review of the topological classification of reflection symmetric semimetals and nodal superconductors [34]. For brevity, we focus on the case where the Fermi surfaces (superconducting nodes) are located within the reflection plane. Second, we discuss in Sec. 3 a four-band tight-binding model on the cubic lattice describing a three-dimensional Dirac semimetal, which is protected by C_4 rotation symmetry. We discuss the surface states of this topological semimetal and determine the symmetries that protect the gapless surface states. Our tight-binding model has similar symmetry properties and topological features as the Dirac semimetal Na_3Bi . Hence, from our topological analysis we can obtain information about the stability of the Fermi arc surface states of Na_3Bi , see Sec. 3.4.

2. Topological classification of reflection symmetric semimetals and nodal superconductors

Before discussing a concrete example of a crystalline topological semimetal, let us briefly review the topological classification of reflection symmetric semimetals and nodal superconductors [34]. The topological properties of reflection symmetric semimetals (nodal superconductors) can be classified in a similar manner as those of reflection symmetric insulators (fully gapped superconductors) [15, 16, 17]. The classification depends on the internal symmetry properties of the nodal system as well as on whether the reflection symmetry commutes or anticommutes with the internal symmetries. There are three fundamental internal symmetries, which act locally in position space, namely time-reversal symmetry (TRS), particle-hole symmetry (PHS), and chiral or sublattice symmetry (SLS). In momentum space, time-reversal and particle-hole symmetry act on the Bloch Hamiltonian $H(\mathbf{k})$ as

$$T^{-1}H(-\mathbf{k})T = +H(\mathbf{k}) \quad (1a)$$

and

$$C^{-1}H(-\mathbf{k})C = -H(\mathbf{k}), \quad (1b)$$

respectively, where $T = \mathcal{K}U_T$ and $C = \mathcal{K}U_C$ are antiunitary operators and \mathcal{K} is the complex conjugation operator. Chiral symmetry is implemented in terms of a unitary matrix S which anti-commutes with the Hamiltonian, i.e., $SH(\mathbf{k}) + H(\mathbf{k})S = 0$.

Crystal reflection symmetry acts non-locally in position space. In the following, we consider a d_{BZ} -dimensional Hamiltonian $H(\mathbf{k})$ which is symmetric under reflection in the first direction.

Hence, $H(\mathbf{k})$ satisfies

$$R^{-1}H(-k_1, \tilde{\mathbf{k}})R = H(k_1, \tilde{\mathbf{k}}), \quad (2)$$

where $\tilde{\mathbf{k}} = (k_2, k_3, \dots, k_{d_{\text{BZ}}})$ and R is a unitary reflection operator. Since a phase factor can be absorbed in the definition of the electron creation and annihilation operators, we can assume that R is Hermitian, i.e., $R^\dagger = R$. As a consequence, the eigenvalues of R are either $+1$ or -1 and all commutation and anti-commutation relations between R and the internal symmetries are defined unambiguously, i.e.,

$$TRT^{-1} = \eta_T R, \quad CRC^{-1} = \eta_C R \quad \text{and} \quad SRS^{-1} = \eta_S R, \quad (3)$$

where the three indices η_T , η_C , and η_S specify whether R commutes ($+1$) or anti-commutes (-1) with the corresponding internal symmetry operator. For the symmetry classes AI, AII, AIII, C, and D these different possibilities are labeled in Table 1 as R_{η_T} , R_{η_C} , and R_{η_S} , respectively. For the symmetry classes that contain two internal symmetries (i.e., classes BDI, CI, CII, and DIII), the different (anti-)commutation relations are denoted by $R_{\eta_T \eta_C}$. Hence, reflection symmetries together with the three internal symmetries define a total of 27 symmetry classes, see Table 1.

The classification of reflection-symmetry-protected semimetals and nodal superconductors depends on the symmetry class and on the codimension of the Fermi surface (superconducting nodes) $p = d_{\text{BZ}} - d_{\text{FS}}$, where d_{BZ} denotes the spatial dimension (i.e., the dimension of the Brillouin zone) and d_{FS} is the dimension of the Fermi surface. Furthermore, the classification depends on how the Fermi surfaces (superconducting nodes) transform under the reflection symmetry and the internal symmetries. In general, one can distinguish three different situations: (i) Each Fermi surface is left invariant by both reflection and internal symmetries, (ii) Fermi surfaces are invariant under reflection symmetry, but are pairwise related to each other by the internal symmetries, and (iii) different Fermi surfaces are pairwise related to each other by both reflection and in internal symmetry operations. In case (i) and case (ii) the Fermi surfaces are located within the reflection plane, whereas in case (iii) the Fermi surfaces are positioned away from the reflection plane. For brevity we focus here on only case (i) and case (ii). Case (iii) has been discussed extensively in Refs. [34] and [36].

2.1. Fermi surfaces at high-symmetry points within mirror plane

First we consider case (i), i.e., Fermi surfaces that are invariant under both reflection and internal symmetries. These Fermi surfaces are located within the reflection plane and at high-symmetry points in the Brillouin zone, that is, at time-reversal invariant momenta. For this case the classification of reflection symmetric Fermi points can be inferred from the classification of reflection-symmetry-protected insulators by means of a dimensional reduction procedure [34]. Namely, the surface states of reflection symmetric d_{BZ} -dimensional topological insulators can be viewed as reflection-symmetry-protected Fermi points in $d_{\text{BZ}} - 1$ dimensions. From this it follows that the topological classification of reflection symmetric Fermi points at time-reversal invariant momenta with $d_{\text{FS}} = 0$ is obtained from the classification of reflection symmetric insulators by the dimensional shift $d_{\text{BZ}} \rightarrow d_{\text{BZ}} - 1$, see Table 1. This logic also works for Fermi surfaces with $d_{\text{FS}} > 0$, if their stability is guaranteed by an $M\mathbb{Z}$ or $2M\mathbb{Z}$ topological number. However, \mathbb{Z}_2 and $M\mathbb{Z}_2$ topological numbers ensure only the stability of Fermi points, i.e., Fermi surfaces with $d_{\text{FS}} = 0$. Derivations based on Clifford analysis and K theory [17, 34] corroborate these findings. The classification of reflection-symmetry-protected Fermi surfaces at high symmetry points of the Brillouin zone is presented in Table 1, where the first row indicates the codimension p of the Fermi surface. We note that the classification is eight-fold periodic in p .

Table 1. Topological classification of reflection-symmetry-protected semimetals and nodal superconductors. The first and second rows specify the codimension $p = d_{\text{BZ}} - d_{\text{FS}}$ of the reflection symmetric Fermi surfaces (superconducting nodes) at high-symmetry points and away from high-symmetry points of the Brillouin zone, respectively. The third row shows the classification of reflection symmetric insulators and fully gapped superconductors [15, 16]. The first column indicates whether the reflection operator R commutes (“ R_+ ”, “ R_{++} ”) or anti-commutes (“ R_- ”, “ R_{--} ”) with the global symmetries. “ R_{+-} ” and “ R_{-+} ” denote the case where R commutes with one of the global symmetries but anti-commutes with the other one. The second column lists the global symmetry classes (using the Cartan nomenclature [3]), which are distinguished by the presence or absence of time-reversal symmetry, particle-hole symmetry, and chiral symmetry.

Reflection	FS in mirror plane at high-sym. point	$p=7$	$p=8$	$p=1$	$p=2$	$p=3$	$p=4$	$p=5$	$p=6$
	FS in mirror plane off high-sym. point	$p=1$	$p=2$	$p=3$	$p=4$	$p=5$	$p=6$	$p=7$	$p=8$
	top. insul. and top. SC	$d_{\text{BZ}}=8$	$d_{\text{BZ}}=1$	$d_{\text{BZ}}=2$	$d_{\text{BZ}}=3$	$d_{\text{BZ}}=4$	$d_{\text{BZ}}=5$	$d_{\text{BZ}}=6$	$d_{\text{BZ}}=7$
R	A	0	$M\mathbb{Z}$	0	$M\mathbb{Z}$	0	$M\mathbb{Z}$	0	$M\mathbb{Z}$
R_+	AIII	$M\mathbb{Z}$	0	$M\mathbb{Z}$	0	$M\mathbb{Z}$	0	$M\mathbb{Z}$	0
R_-	AIII	0	$M\mathbb{Z} \oplus \mathbb{Z}$	0	$M\mathbb{Z} \oplus \mathbb{Z}$	0	$M\mathbb{Z} \oplus \mathbb{Z}$	0	$M\mathbb{Z} \oplus \mathbb{Z}$
R_+, R_{++}	AI	$M\mathbb{Z}_2^{a,b}$	$M\mathbb{Z}$	0	0	0	$2M\mathbb{Z}$	0	$M\mathbb{Z}_2^{a,b}$
	BDI	$M\mathbb{Z}_2^{a,b}$	$M\mathbb{Z}_2^{a,b}$	$M\mathbb{Z}$	0	0	0	$2M\mathbb{Z}$	0
	D	0	$M\mathbb{Z}_2^{a,b}$	$M\mathbb{Z}_2^{a,b}$	$M\mathbb{Z}$	0	0	0	$2M\mathbb{Z}$
	DIII	$2M\mathbb{Z}$	0	$M\mathbb{Z}_2^{a,b}$	$M\mathbb{Z}_2^{a,b}$	$M\mathbb{Z}$	0	0	0
	AII	0	$2M\mathbb{Z}$	0	$M\mathbb{Z}_2^{a,b}$	$M\mathbb{Z}_2^{a,b}$	$M\mathbb{Z}$	0	0
	CII	0	0	$2M\mathbb{Z}$	0	$M\mathbb{Z}_2^{a,b}$	$M\mathbb{Z}_2^{a,b}$	$M\mathbb{Z}$	0
	C	0	0	0	$2M\mathbb{Z}$	0	$M\mathbb{Z}_2^{a,b}$	$M\mathbb{Z}_2^{a,b}$	$M\mathbb{Z}$
	CI	$M\mathbb{Z}$	0	0	0	$2M\mathbb{Z}$	0	$M\mathbb{Z}_2^{a,b}$	$M\mathbb{Z}_2^{a,b}$
R_-, R_{--}	AI	0	0	0	$2M\mathbb{Z}$	0	$T\mathbb{Z}_2^{a,b,c}$	$\mathbb{Z}_2^{a,b}$	$M\mathbb{Z}$
	BDI	$M\mathbb{Z}$	0	0	0	$2M\mathbb{Z}$	0	$T\mathbb{Z}_2^{a,b,c}$	$\mathbb{Z}_2^{a,b}$
	D	$\mathbb{Z}_2^{a,b}$	$M\mathbb{Z}$	0	0	0	$2M\mathbb{Z}$	0	$T\mathbb{Z}_2^{a,b,c}$
	DIII	$T\mathbb{Z}_2^{a,b,c}$	$\mathbb{Z}_2^{a,b}$	$M\mathbb{Z}$	0	0	0	$2M\mathbb{Z}$	0
	AII	0	$T\mathbb{Z}_2^{a,b,c}$	$\mathbb{Z}_2^{a,b}$	$M\mathbb{Z}$	0	0	0	$2M\mathbb{Z}$
	CII	$2M\mathbb{Z}$	0	$T\mathbb{Z}_2^{a,b,c}$	$\mathbb{Z}_2^{a,b}$	$M\mathbb{Z}$	0	0	0
	C	0	$2M\mathbb{Z}$	0	$T\mathbb{Z}_2^{a,b,c}$	$\mathbb{Z}_2^{a,b}$	$M\mathbb{Z}$	0	0
	CI	0	0	$2M\mathbb{Z}$	0	$T\mathbb{Z}_2^{a,b,c}$	$\mathbb{Z}_2^{a,b}$	$M\mathbb{Z}$	0
R_{+-}	BDI, CII	0	$2\mathbb{Z}$	0	$2M\mathbb{Z}$	0	$2\mathbb{Z}$	0	$2M\mathbb{Z}$
R_{-+}	DIII, CI	0	$2M\mathbb{Z}$	0	$2\mathbb{Z}$	0	$2M\mathbb{Z}$	0	$2\mathbb{Z}$
R_{+-}	BDI	$M\mathbb{Z}_2 \oplus \mathbb{Z}_2^{a,b}$	$M\mathbb{Z} \oplus \mathbb{Z}$	0	0	0	$2M\mathbb{Z} \oplus 2\mathbb{Z}$	0	$M\mathbb{Z}_2 \oplus \mathbb{Z}_2^{a,b}$
R_{-+}	DIII	0	$M\mathbb{Z}_2 \oplus \mathbb{Z}_2^{a,b}$	$M\mathbb{Z}_2 \oplus \mathbb{Z}_2^{a,b}$	$M\mathbb{Z} \oplus \mathbb{Z}$	0	0	0	$2M\mathbb{Z} \oplus 2\mathbb{Z}$
R_{+-}	CII	0	$2M\mathbb{Z} \oplus 2\mathbb{Z}$	0	$M\mathbb{Z}_2 \oplus \mathbb{Z}_2^{a,b}$	$M\mathbb{Z}_2 \oplus \mathbb{Z}_2^{a,b}$	$M\mathbb{Z} \oplus \mathbb{Z}$	0	0
R_{-+}	CI	0	0	0	$2M\mathbb{Z} \oplus 2\mathbb{Z}$	0	$M\mathbb{Z}_2 \oplus \mathbb{Z}_2^{a,b}$	$M\mathbb{Z}_2 \oplus \mathbb{Z}_2^{a,b}$	$M\mathbb{Z} \oplus \mathbb{Z}$

^a \mathbb{Z}_2 and $M\mathbb{Z}_2$ invariants only protect Fermi surfaces of dimension zero (i.e., Fermi points with $d_{\text{FS}} = 0$) at high-symmetry points of the Brillouin zone.

^b Fermi surfaces located within the mirror plane but away from high symmetry points cannot be protected by a \mathbb{Z}_2 or $M\mathbb{Z}_2$ topological number. However, the nodal system can exhibit zero-energy surface states that are protected by a \mathbb{Z}_2 or $M\mathbb{Z}_2$ topological number.

^c For topological semimetals (nodal topological superconductors) the presence of translation symmetry is always assumed. Therefore, one does not need to distinguish between $T\mathbb{Z}_2$ and \mathbb{Z}_2 invariants for these gapless topological materials.

2.2. Fermi surfaces within mirror plane but off high-symmetry points

Second, we review case (ii), i.e., the classification of reflection symmetric Fermi surfaces that are located away from high-symmetry points of the Brillouin zone. These Fermi surfaces transform pairwise into each other by the global (i.e., internal) symmetries, which relate $\mathbf{k} \rightarrow -\mathbf{k}$. Using an analysis based on the minimal-Dirac-Hamiltonian method, it was show in Ref. [34] that only $M\mathbb{Z}$ and $2M\mathbb{Z}$ topological numbers can ensure the stability of reflection symmetric Fermi surfaces off high-symmetry points. \mathbb{Z}_2 and $M\mathbb{Z}_2$ invariants, on the other hand, do not give rise to stable Fermi surfaces. However, as illustrated in Sec. 3, \mathbb{Z}_2 or $M\mathbb{Z}_2$ invariants may nevertheless lead to protected zero-energy surface states at time-reversal-invariant momenta of the surface Brillouin zone. The classification of reflection symmetric Fermi surfaces located away from high-symmetry points is summarized in Table 1. As above, we note that due to Bott’s periodicity theorem [50], the classification scheme exhibits an eight-fold periodicity in p . We observe that the classification of reflection-symmetric Fermi surfaces located away from high symmetry points

with codimension p is related to the classification of reflection-symmetric insulators with spatial dimension $d_{\text{BZ}} = p - 1$.

3. Topological Dirac semimetal with reflection and rotation symmetry

In this section we discuss a tight-binding model describing a topological semimetal which exhibits time-reversal symmetry as well as reflection and rotation symmetries. This model is inspired by the Dirac material Na_3Bi , whose three-dimensional bulk Dirac cones are protected by reflection symmetry. Using angle-resolved photoemission experiments, topological surface modes have recently been observed on the (100) surface of Na_3Bi [49].

3.1. Model Hamiltonian

We consider the following cubic-lattice Hamiltonian describing a four-band semimetal with two Dirac points

$$\hat{H} = \frac{1}{2} \sum_{\vec{x}} \left[C_{\vec{x}+\hat{x}}^\dagger (\tau_z s_0 + i\tau_x s_x) C_{\vec{x}} + C_{\vec{x}+\hat{y}}^\dagger (\tau_z s_0 + i\tau_x s_y) C_{\vec{x}} + C_{\vec{x}+\hat{z}}^\dagger \tau_z s_0 C_{\vec{x}} + m C_{\vec{x}}^\dagger \tau_z s_0 C_{\vec{x}} \right] + \text{h.c.}, \quad (4a)$$

with the spinor $C_{\vec{x}} = [c_{1\uparrow}(\vec{x}), c_{1\downarrow}(\vec{x}), c_{2\uparrow}(\vec{x}), c_{2\downarrow}(\vec{x})]$, where $c_{n\sigma}(\vec{x})$ denotes the electron annihilation operator with orbital index n and spin σ . The two sets of Pauli matrices τ_α and s_α operate in spin space and orbital space, respectively. In momentum space Hamiltonian (4a) takes diagonal form $\mathcal{H} = \sum_{\mathbf{k}} C_{\mathbf{k}}^\dagger H(\mathbf{k}) C_{\mathbf{k}}$, with $C_{\mathbf{k}}$ the Fourier-transformed spinor, and

$$H(\mathbf{k}) = \sin k_x \tau_x s_x + \sin k_y \tau_y s_y + (\cos k_x + \cos k_y + \cos k_z - m) \tau_z s_0. \quad (4b)$$

For concreteness we set $m = 2$. With this choice, the bulk Dirac cones of $H(\mathbf{k})$ are positioned at $\mathbf{k}_\pm = (0, 0, \pm\pi/2)$, i.e., they are located on the k_z axis just as in the Dirac material Na_3Bi . The cubic-lattice Hamiltonian (4b) possesses a rotation symmetry of order four about the z axis. This C_4 rotation symmetry acts on $H(\mathbf{k})$ as

$$R_{C_4}^{-1} H(-k_y, k_x, k_z) R_{C_4} = H(k_x, k_y, k_z), \quad (5)$$

where $R_{C_4} = \tau_z(s_0 + is_z)/\sqrt{2}$ denotes the C_4 rotation operator. The Dirac semimetal (4) also preserves time reversal symmetry, Eq. (1a), with the time-reversal operator $T = \tau_0 s_y \mathcal{K}$. Since $T^2 = -\mathbb{1}$, Hamiltonian (4) belongs to symmetry class AII. The codimension of the Dirac cones of $H(\mathbf{k})$, which are located away from the high symmetry points in the Brillouin zone, is $p = 3$. Hence, according to the classification of Ref. [34] (see Table 1 in Ref. [34]), the Dirac points are not protected by time-reversal symmetry, even though a binary \mathbb{Z}_2 invariant can be defined for this symmetry class. (As we will show below, this \mathbb{Z}_2 invariant leads to gapless surface states at time-reversal-invariant momenta of the surface Brillouin zone.) Indeed, we find that the bulk Dirac cones can be gapped out by the mass term $\sin k_z \tau_y s_0$, which preserves time reversal symmetry. However, the mass term $\sin k_z \tau_y s_0$ breaks the C_4 rotation symmetry (5). In general, we find that the only possible gap opening terms are $f_1(k_z) \tau_y s_0$ and $f_2(k_z) \tau_x s_z$, since these are the terms that anti-commute with $H(\mathbf{k})$. Here, $f_1(k_z)$ and $f_2(k_z)$ represent k_z dependent masses. We find that these two gap opening terms break the C_4 rotation symmetry (5), since they anti-commute with R_{C_4} . As a consequence, the two Dirac cones of Hamiltonian (4) are protected against gap opening by the C_4 rotation symmetry (5).

3.2. Surface states

As discussed above and in Ref. [34], class AII Dirac points with codimension $p = 3$ that are located away from high-symmetry points of the Brillouin zone are unstable in the absence of

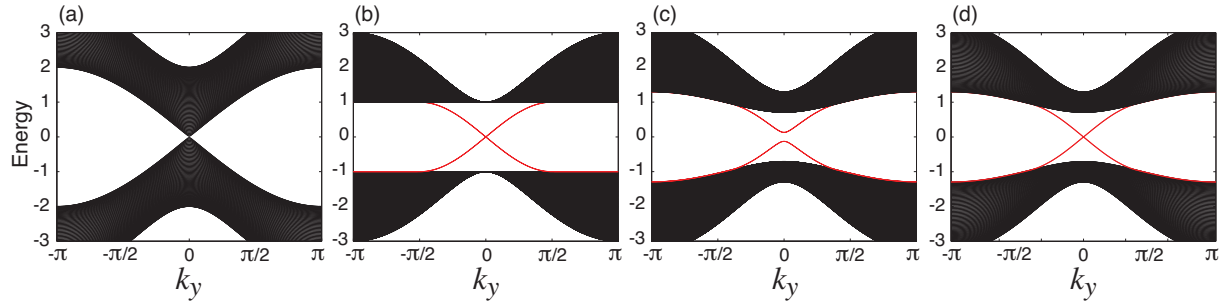


Figure 1. (a) Surface band structure of the Dirac semimetal (4) for a (100) slab as a function of surface momentum k_y with fixed $k_z = \pi/2$. (b) Same as panel (a) but for $k_z = 0$. The gapless surface state at $k_y = 0$ is protected by a \mathbb{Z}_2 invariant. (c) Band structure at the (100) surface of the Dirac semimetal (8) as a function of k_y with $k_z = \pi/4$. In the absence of reflection symmetry (6) and chiral symmetry (7) the surface state (red trace) is gapped. (d) Surface band structure of the Dirac semimetal (4) (i.e., with reflection symmetry and chiral symmetry) as a function of k_y with $k_z = \pi/4$.

crystal lattice symmetries, even though a binary \mathbb{Z}_2 index can be defined for this symmetry class. This \mathbb{Z}_2 invariant does not guarantee the stability of Dirac points, however it gives rise to protected gapless surface states at time-reversal invariant momenta of the surface Brillouin zone. For the Dirac semimetal (4) these gapless modes appear at $(k_y, k_z) = (0, 0)$ of the (100) surface Brillouin zone, see Fig. 1(b). For other surface momenta, the surface states are in general gapped. Similarly, rotation symmetry (5) can protect surface states only at time-reversal-invariant momenta of the surface Brillouin zone, but not away from these points.

To illustrate this, we consider Hamiltonian (4) with periodic boundary conditions along the z -axis and open boundary conditions along the x - and y -directions. We observe that model Hamiltonian (4) exhibits besides rotation symmetry (5) an *accidental* reflection symmetry

$$R_y^{-1} H(k_x, -k_y, k_z) R_y = H(k_x, k_y, k_z), \quad (6)$$

with $R_y = \tau_z s_y$, and an *accidental* chiral symmetry

$$H(\mathbf{k}) S = -S H(\mathbf{k}), \quad (7)$$

with $S = \tau_x s_z$. In order to break these accidental symmetries we need to add to the Hamiltonian the term $+g \sin k_z \tau_x s_z$ on the (100) and $(\bar{1}00)$ surfaces, and the term $-g \sin k_z \tau_x s_z$ on the (010) and $(0\bar{1}0)$ surfaces. That is, we consider

$$\tilde{H}(k_z) = \hat{H}(k_z) + g \sum_{\vec{x}_\perp} C_{\vec{x}_\perp}^\dagger \sin k_z \tau_x s_z \left[\delta_{\vec{x}_\perp, \vec{x}_\perp^{(100)}} + \delta_{\vec{x}_\perp, \vec{x}_\perp^{(\bar{1}00)}} - \delta_{\vec{x}_\perp, \vec{x}_\perp^{(010)}} - \delta_{\vec{x}_\perp, \vec{x}_\perp^{(0\bar{1}0)}} \right] C_{\vec{x}_\perp}, \quad (8)$$

where $\hat{H}(k_z)$ is obtained from Eq. (4a) by Fourier transforming the z -coordinate and the sum in Eq. (8) is over a collection of one-dimensional chains which are oriented along the z -axis and labeled by \vec{x}_\perp . Hamiltonian (8) is symmetric under time-reversal symmetry and rotation symmetry (5), but breaks the accidental symmetries (6) and (7). Fig. 1(c) shows the (100) surface spectrum of Hamiltonian (8) with $g = 0.2$ as a function of surface momentum k_y for $k_z = \pi/4$. Fig. 2(a) displays the (100) surface spectrum as a function of both surface momenta k_y and k_z . We observe that the surface state is gapped, except at $(k_y, k_z) = (0, 0)$, where it is protected by time-reversal symmetry (i.e., the aforementioned \mathbb{Z}_2 invariant).

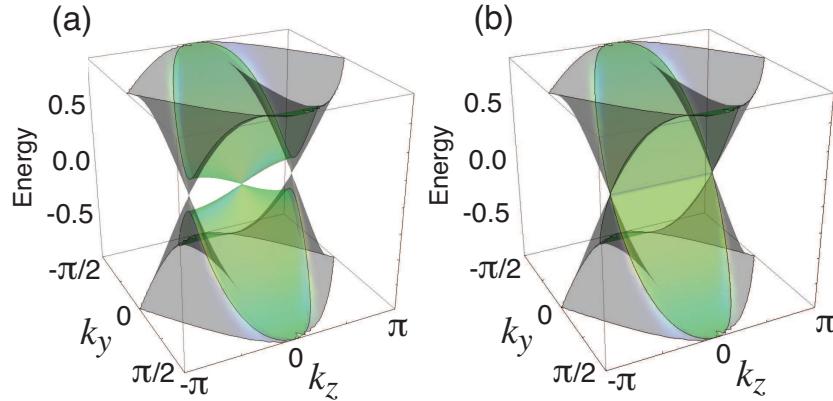


Figure 2. (a) Surface spectrum of the Dirac semimetal (8) for the (100) face as a function of surface momenta k_y and k_z . The surface states and bulk states are colored in green and gray, respectively. In the absence of reflection symmetry (6) and chiral symmetry (7) the surface state is gapped except at $(k_y, k_z) = (0, 0)$. (b) Surface spectrum of the Dirac semimetal (4), i.e., in the presence of reflection symmetry and chiral symmetry. The gaplessness of the Fermi arc is guaranteed by the mirror winding number (9).

On the other hand, if we consider a semimetal which possesses also symmetries (6) and (7) [i.e., Hamiltonian (4) instead of Hamiltonian (8)], then the surface states are gapless along a one-dimensional arc that connects the two projected Dirac nodes $\mathbf{k}_{\pm} = (0, 0, \pm\pi/2)$, see Fig. 1(d) and Fig. 2(b). Since the reflection operator R_y anti-commutes with the time-reversal operator $T = \tau_0 s_y \mathcal{K}$ and with the effective particle-hole operator $C = T^{-1}S = i\tau_x s_x \mathcal{K}$, Hamiltonian (4) can be viewed as a member of symmetry class DIII with R_{--} in Table 1. Hence, according to the classification scheme of Sec. 2.2 the Dirac nodes of Eq. (4) are protected by an $M\mathbb{Z}$ invariant, i.e., a mirror winding number. Moreover, Hamiltonian (4) exhibits Fermi arc surface states, which are protected by this mirror winding number. This mirror invariant is defined in terms of a one-dimensional integral along a contour that lies within the mirror plane $k_y = 0$. Within the $k_y = 0$ mirror plane the Hamiltonian can be block diagonalized with respect to R_y . For the block with mirror eigenvalue $R_y = +1$ the mirror winding number takes the form

$$n_C^+ = \frac{i}{2\pi} \int_C \text{Tr}(q^* dq), \quad \text{with} \quad q = \frac{\sin k_x - iM(k_x)}{\sin^2 k_x + M^2(k_x)} \quad (9)$$

and $M(k_x) = \cos k_x + \cos k_z - 1$, where \mathcal{C} denotes a contour that lies within the mirror plane. Choosing the contour \mathcal{C} to be parallel to the k_x -axis with $k_y = 0$ and k_z a fixed parameter we find that

$$n^+(k_z) = \begin{cases} -1, & |k_z| < \pi/2 \\ 0, & |k_z| > \pi/2 \end{cases} \quad (10)$$

This indicates that there exists a gapless Fermi arc state at $k_y = 0$ on the (100) surface, which is in agreement with the spectrum shown in Fig. 2(b).

3.3. The role of translation symmetry

While each Dirac point of a topological semimetal is stable against deformations that are local in momentum space, the Dirac points are not protected against commensurate perturbations, such as charge-density wave modulations, which connect Dirac points with opposite momenta.

However, these deformations are forbidden, if we impose besides internal and crystal point-group symmetries, also translation symmetry.

To illustrate the instability of the Dirac points against charge-density wave perturbations, let us consider a low-energy description of semimetal (4). Expanding Eq. (4) around the two Dirac points $\mathbf{k}_\pm = (0, 0, \pm\pi/2)$, we obtain the following low-energy effective Hamiltonian

$$\hat{H}_{\text{eff}} = \sum_{k_x, k_y, k_\Delta} \begin{pmatrix} C_{\mathbf{K}_+}^\dagger & C_{\mathbf{K}_-}^\dagger \end{pmatrix} \begin{pmatrix} h_+ & 0 \\ 0 & h_- \end{pmatrix} \begin{pmatrix} C_{\mathbf{K}_+} \\ C_{\mathbf{K}_-} \end{pmatrix}, \quad (11)$$

where $\mathbf{K}_\pm = (k_x, k_y, k_\Delta \pm \pi/2)$ and $h_\pm = k_x \tau_x s_x + k_y \tau_y s_y \mp k_\Delta \tau_z s_0$. Hamiltonian \hat{H}_{eff} is symmetric under the C_4 rotation symmetry (5), which transforms $C_{\mathbf{K}_\pm} \rightarrow \tau_z(s_0 + i s_z) C_{\tilde{\mathbf{K}}_\pm} / \sqrt{2}$, and the time reversal symmetry (1a), which transforms $C_{\mathbf{K}_\pm} \rightarrow \tau_0 s_y \mathcal{K} C_{-\mathbf{K}_\pm}$. We find that the two Dirac cones can be gapped out by the charge-density wave modulation

$$\hat{D} = \sum_{k_x, k_y, k_\Delta} \begin{pmatrix} C_{\mathbf{K}_+}^\dagger & C_{\mathbf{K}_-}^\dagger \end{pmatrix} \begin{pmatrix} 0 & \tau_z s_0 \\ \tau_z s_0 & 0 \end{pmatrix} \begin{pmatrix} C_{\mathbf{K}_+} \\ C_{\mathbf{K}_-} \end{pmatrix}, \quad (12)$$

which preserves rotation symmetry (5), but breaks translation symmetry. We conclude that in the absence of translation symmetry, the Dirac cones of semimetals are unstable against charge-density wave-type perturbations.

3.4. Implications for Na_3Bi

Albeit Na_3Bi has hexagonal $P6_3/mmc$ crystal structure rather than cubic one, its topological and symmetry properties are similar to the model Hamiltonian (8). Instead of C_4 rotation symmetry, Na_3Bi exhibits a C_3 rotation symmetry, which protects the two gapless bulk Dirac cones. Using a downfolding procedure, it is possible to derive from DFT band structure calculations a low-energy hexagonal-lattice tight-binding model for Na_3Bi . This tight-binding model is expected to exhibit similar symmetry properties and the same topological features as our tight-binding Hamiltonian (8). Hence, this suggests that Na_3Bi supports Fermi arc surface states, which are gapped except at time-reversal invariant points of the surface Brillouin zone. This expectation is confirmed by recent angle-resolved photoemission experiments [48, 49].

4. Summary and discussion

In this paper, we have reviewed the topological classification of reflection-symmetry-protected semimetals and nodal superconductors. This classification scheme depends on (i) the internal symmetry properties of the Hamiltonian, (ii) whether the reflection symmetry commutes or anti-commutes with the internal symmetries, (iii) the codimension of the Fermi surface (superconducting node) $p = d_{\text{BZ}} - d_{\text{FS}}$, and (iv) the transformation properties of the Fermi surface (superconducting node) under the action of the reflection and internal symmetries. Reflection symmetry together with the internal (i.e., non-spatial) symmetries define a total of 27 symmetry classes. The result of the classification scheme is presented in Table 1. The stability of the Fermi surface is ensured by the conservation of a topological invariant that is defined as an integral along a contour surrounding the Fermi surface. These topological numbers can be Chern or winding numbers (indicated by “ \mathbb{Z} ” in Table 1), binary invariants (indicated by “ \mathbb{Z}_2 ”), mirror Chern or mirror winding numbers (indicated by “ $M\mathbb{Z}$ ”), or mirror binary invariants (indicated by “ $M\mathbb{Z}_2$ ”).

To illustrate the usefulness of the classification Table 1, we have discussed in Sec. 3 an example of a topological semimetal with time-reversal symmetry and rotation symmetry. This model Hamiltonian represents a cubic lattice version of the hexagonal Dirac material Na_3Bi . We

determined the surface state spectrum of this Dirac model system and discussed its topological properties. We found that the (100) surface supports Fermi arc surface states, which are gapped except at the $\bar{\Gamma}$ point of the surface Brillouin zone, see Fig. 2(a). This is in agreement with recent angular-resolved photoemission experiments on the (100) surface of Na₃Bi [48, 49].

Acknowledgments

The authors thank Wei-Feng Tsai for useful discussions. The support of the Max-Planck-UBC Centre for Quantum Materials is gratefully acknowledged.

References

- [1] Schnyder A P, Ryu S, Furusaki A and Ludwig A W W 2008 *Phys. Rev. B* **78** 195125
- [2] Kitaev A 2009 *AIP Conf. Proc.* **1134** 22
- [3] Schnyder A P, Ryu S, Furusaki A and Ludwig A W W 2009 *AIP Conf. Proc.* **1134** 10
- [4] Ryu S, Schnyder A P, Furusaki A and Ludwig A W W 2010 *New J. Phys.* **12** 065010
- [5] Chiu C K 2014 *ArXiv e-prints (Preprint 1410.1117)*
- [6] Teo J C Y, Fu L and Kane C L 2008 *Phys. Rev. B* **78** 045426
- [7] Fu L 2011 *Phys. Rev. Lett.* **106** 106802
- [8] Slager R J, Mesaros A, Juricic V and Zaanen J 2013 *Nat. Phys.* **9** 98
- [9] Ueno Y, Yamakage A, Tanaka Y and Sato M 2013 *Phys. Rev. Lett.* **111** 087002
- [10] Zhang F, Kane C L and Mele E J 2013 *Phys. Rev. Lett.* **111** 056403
- [11] Benalcazar W A, Teo J C Y and Hughes T L 2014 *Phys. Rev. B* **89**(22) 224503
- [12] Teo J C Y and Hughes T L 2013 *Phys. Rev. Lett.* **111**(4) 047006
- [13] Turner A M, Zhang Y, Mong R S K and Vishwanath A 2012 *Phys. Rev. B* **85** 165120
- [14] Hughes T L, Prodan E and Bernevig B A 2011 *Phys. Rev. B* **83** 245132
- [15] Chiu C K, Yao H and Ryu S 2013 *Phys. Rev. B* **88**(7) 075142
- [16] Morimoto T and Furusaki A 2013 *Phys. Rev. B* **88**(12) 125129
- [17] Shiozaki K and Sato M 2014 *Phys. Rev. B* **90**(16) 165114
- [18] Tanaka Y, Ren Z, Sato T, Nakayama K, Souma S, Takahashi T, Segawa K and Ando Y 2012 *Nat Phys* **8** 800
- [19] Hsieh T H, Lin H, Liu J, Duan W, Bansil A and Fu L 2012 *Nat. Commun.* **3** 982
- [20] Xu S Y, Liu C, Alidoust N, Neupane M, Qian D, Belopolski I, Denlinger J D, Wang Y J, Lin H, Wray L A, Landolt G, Slomski B, Dil J H, Marcinkova A, Morosan E, Gibson Q, Sankar R, Chou F C, Cava R J, Bansil A and Hasan M Z 2012 *Nat. Commun.* **3** 1192
- [21] Dziawa *et al* P 2012 *Nat. Mater.* **11** 1023
- [22] Kariyado T and Ogata M 2011 *Journal of the Physical Society of Japan* **80** 083704
- [23] Kariyado T and Ogata M 2012 *Journal of the Physical Society of Japan* **81** 064701
- [24] Hsieh T H, Liu J W and Fu L 2014 *Phys. Rev. B* **90** 08112
- [25] Béri B 2010 *Phys. Rev. B* **81**(13) 134515
- [26] Wan X, Turner A M, Vishwanath A and Savrasov S Y 2011 *Phys. Rev. B* **83**(20) 205101
- [27] Schnyder A P and Ryu S 2011 *Phys. Rev. B* **84**(6) 060504
- [28] Brydon P M R, Schnyder A P and Timm C 2011 *Phys. Rev. B* **84**(2) 020501
- [29] Schnyder A P, Brydon P M R and Timm C 2011 *Phys. Rev. B* **85** 24522
- [30] Matsuura S, Chang P Y, Schnyder A P and Ryu S 2013 *New J. Phys.* **15** 065001
- [31] Zhao Y X and Wang Z D 2013 *Phys. Rev. Lett.* **110**(24) 240404
- [32] Zhao Y X and Wang Z D 2014 *Phys. Rev. B* **89**(7) 075111
- [33] Turner A M and Vishwanath A 2013 *ArXiv e-prints (Preprint 1301.0330)*
- [34] Chiu C K and Schnyder A P 2014 *Phys. Rev. B* **90**(20) 205136
- [35] Yang B J and Nagaosa N 2014 *Nat. Commun.* **5** 4898
- [36] Morimoto T and Furusaki A 2014 *Phys. Rev. B* **89**(23) 235127
- [37] Chang P Y, Matsuura S, Schnyder A P and Ryu S 2014 *Phys. Rev. B* **90**(17) 174504
- [38] Chen Y, Lu Y M and Kee H Y 2014 *ArXiv e-prints (Preprint 1410.5830)*
- [39] Jeon S, Zhou B B, Gyenis A, Feldman B E, Kimchi I, Potter A C, Gibson Q D, Cava R J, Vishwanath A and Yazdani A 2014 *Nat. Mater.* **13** 851
- [40] Wang Z, Weng H, Wu Q, Dai X and Fang Z 2013 *Phys. Rev. B* **88**(12) 125427
- [41] Neupane M, Xu S Y, Sankar R, Alidoust N, Bian G, Liu C, Belopolski I, Chang T R, Jeng H T, Lin H, Bansil A, Chou F and Hasan M Z 2014 *Nat. Commun.* **5** 3786

- [42] Borisenko S, Gibson Q, Evtushinsky D, Zabolotnyy V, Büchner B and Cava R J 2014 *Phys. Rev. Lett.* **113**(2) 027603
- [43] Liu Z K, Jiang J, Zhou B, Wang Z J, Zhang Y, Weng H M, Prabhakaran D, Mo S K, Peng H, Dudin P, Kim T, Hoesch M, Fang Z, Dai X, Shen Z X, Feng D L, Hussain Z and Chen Y L 2014 *Nat. Mater.* **13** 677
- [44] He L P, Hong X C, Dong J K, Pan J, Zhang Z, Zhang J and Li S Y 2014 *Phys. Rev. Lett.* **113**(24) 246402
- [45] Liang T, Gibson Q, Ali M N, Liu M, Cava R J and Ong N P 2014 *Nature Materials* (Preprint <http://nmat/journal/vaop/ncurrent/full/nmat4143.html>)
- [46] Liu Z K, Zhou B, Zhang Y, Wang Z J, Weng H M, Prabhakaran D, Mo S K, Shen Z X, Fang Z, Dai X, Hussain Z and Chen Y L 2014 *Science* **343** 864
- [47] Wang Z, Sun Y, Chen X Q, Franchini C, Xu G, Weng H, Dai X and Fang Z 2012 *Phys. Rev. B* **85**(19) 195320
- [48] Xu S Y, Liu C, Kushwaha S K, Chang T R, Krizan J W, Sankar R, Polley C M, Adell J, Balasubramanian T, Miyamoto K, Alidoust N, Bian G, Neupane M, Belopolski I, Jeng H T, Huang C Y, Tsai W F, Lin H, Chou F C, Okuda T, Bansil A, Cava R J and Hasan M Z 2013 *ArXiv e-prints* (Preprint 1312.7624)
- [49] Xu S Y, Liu C, Kushwaha S K, Sankar R, Krizan J W, Belopolski I, Neupane M, e, Bian G, Alidoust N, Chang T R, Jeng H T, Huang C Y, Tsai W F, Lin H, Shibaev P P, Chou F, Cava R J and Hasan M Z 2014 *Science* (Preprint <http://www.sciencemag.org/content/early/2014/12/17/science.1256742.full.pdf>)
- [50] Bott R 1970 *Advances in Mathematics* **4** 353